Human Molecular Genetics, 2017, Vol. 26, No. 21 4278–4289

doi: 10.1093/hmg/ddx316
Advance Access Publication Date: 16 August 2017
Original Article

ORIGINAL ARTICLE

Identification of a novel synaptic protein, TMTC3, involved in periventricular nodular heterotopia with intellectual disability and epilepsy

Sali M.K. Farhan[1,2], Kevin C.J. Nixon[3], Michelle Everest[1,3], Tara N. Edwards[3], Shirley Long[3], Dmitri Segal[3], Maria J. Knip[3], Heleen H. Arts[1,4,5], Rana Chakrabarti[4,6], Jian Wang[1], John F. Robinson[1], Donald Lee[7], Seyed M. Mirsattari[3,8], C. Anthony Rupar[2,4,6,9], Victoria M. Siu[2,4,6], FORGE Canada Consortium, Michael O. Poulter[1,3], Robert A. Hegele[1,2] and Jamie M. Kramer[3,4,10,*]

[1]Molecular Medicine Research Group, Robarts Research Institute, London, ON, Canada, N6A 5B7, [2]Department of Biochemistry, [3]Department of Physiology and Pharmacology, Schulich School of Medicine and Dentistry, Western University, London, ON, Canada, N6A 5C1, [4]Division of Genetics and Development, Children's Health Research Institute, London, ON, Canada, N6A 5W9, [5]Department of Human Genetics, Radboud Institute for Molecular Life Sciences, Radboud University Medical Centre Nijmegen, The Netherlands, [6]Department of Pediatrics, [7]Department of Medical Imaging, [8]Departments of Clinical Neurological Sciences, Medical Biophysics, Medical Imaging and Psychology, [9]Department of Pathology and Laboratory Medicine, Schulich School of Medicine and Dentistry, Western University, London, ON, Canada, N6A 5C1 and [10]Department of Biology, Faculty of Science, Western University, London, ON, Canada, N6A 5B7

*To whom correspondence should be addressed at: Department of Physiology and Pharmacology, Schulich School of Medicine & Dentistry, Western University, Medical Sciences Building, Room 266, London, ON, Canada, N6A 5C1. Tel: 519-661-3740; Fax: 519-661-3827; Email: James.Kramer@schulich.uwo.ca

Abstract

Defects in neuronal migration cause brain malformations, which are associated with intellectual disability (ID) and epilepsy. Using exome sequencing, we identified compound heterozygous variants (p.Arg71His and p. Leu729ThrfsTer6) in *TMTC3*, encoding transmembrane and tetratricopeptide repeat containing 3, in four siblings with nocturnal seizures and ID. Three of the four siblings have periventricular nodular heterotopia (PVNH), a common brain malformation caused by failure of neurons to migrate from the ventricular zone to the cortex. Expression analysis using patient-derived cells confirmed reduced *TMTC3* transcript levels and loss of the TMTC3 protein compared to parental and control cells. As TMTC3 function is currently unexplored in the brain, we gathered support for a neurobiological role for TMTC3 by generating flies with post-mitotic neuron-specific knockdown of the highly conserved *Drosophila melanogaster* TMTC3 ortholog, *CG4050/tmtc3*. Neuron-specific knockdown of *tmtc3* in flies resulted in increased susceptibility to induced seizures. Importantly, this phenotype was rescued by neuron-specific

Received: March 29, 2017. **Revised:** June 29, 2017. **Accepted:** August 8, 2017

expression of human *TMTC3*, suggesting a role for TMTC3 in seizure biology. In addition, we observed co-localization of TMTC3 in the rat brain with vesicular GABA transporter (VGAT), a presynaptic marker for inhibitory synapses. TMTC3 is localized at VGAT positive pre-synaptic terminals and boutons in the rat hypothalamus and piriform cortex, suggesting a role for TMTC3 in the regulation of GABAergic inhibitory synapses. TMTC3 did not co-localize with Vglut2, a presynaptic marker for excitatory neurons. Our data identified TMTC3 as a synaptic protein that is involved in PVNH with ID and epilepsy, in addition to its previously described association with cobblestone lissencephaly.

Introduction

Many neurodevelopmental disorders associated with epilepsy and intellectual disability (ID) are caused by defects in neuronal migration, which result in brain malformations such as lissencephaly, pachygyria, polymicrogyria, and periventricular nodular heterotopias (PVNHs) (1). PVNH is one of the most common brain malformations, and is caused by the failure of neurons to migrate from the ventricular zone to the cortex during early brain development (2). PVNH has been linked to mutations in *FLNA* (OMIM 300049) (3), *ARFGEF2* (OMIM 608097) (4), *ERMARD* (OMIM 615544) (5), and *NEDD4L* (OMIM 617201) (6). Functional investigation of these causative genes suggests that PVHN may result from disrupted cytoskeletal dynamics and vesicular trafficking (7). PVNH-causing mutations in NEDD4L have been shown to cause deregulation of Akt and mTor signaling (6). Despite these advances, the mechanisms underlying PVNH are still not well understood, and most cases have no genetic diagnosis.

Recently, the *transmembrane and tetratricopeptide repeat containing 3* (*TMTC3*) gene was implicated in a neuronal migration defect leading to cobblestone lissencephaly (COB), a cortical malformation caused by over migration of neurons beyond the basement membrane. Here, we show that loss of TMTC3 also causes PVNH, in a family with four affected siblings presenting with nocturnal seizures and ID. Furthermore, we demonstrate a neuron-specific role for TMTC3 in mechanically induced seizures in *Drosophila*, and provide evidence for synaptic localization of TMTC3 in the mammalian brain.

Results

Clinical description of patients with nocturnal seizures and ID

Four siblings, three females and one male, the only children born to a healthy non-consanguineous Pakistani couple (Fig. 1A), have a similar history of mild to moderate ID and recurrent nocturnal seizures, with onset between one and four years of age (Table 1). The seizures start with upper respiratory airway obstruction, followed by tonic stiffening and coarse tremor of the limbs. Episodes typically last less than 1–2 min and can occur up to 4 times per night, up to 4 to 5 days a week. There is no history of diurnal or photic-induced seizures, except for few rare seizures during the day in II-2. Seizure frequency has decreased with age and on various combinations of carbamazepine, lamotrigine, valproic acid, and clobazam. Currently, at ages ranging between 21 and 30 years, all have been seizure-free for at least a year.

All four siblings were born at term and apparently had normal gross motor development with sitting and walking achieved by 1 year. Three of the four began talking at 1 year, but II-3 did not talk until 4 years. There were cognitive delays from early childhood, with no regression in skills. The two older siblings can read. II-3 and II-4 have behavioral problems consisting of aggression, agitation, irritability, and self-harm. All 4 siblings are bilingual in English and Urdu, and can express themselves to a greater or lesser degree and follow simple instructions. They are all capable of activities of daily living. Subject II-2, whose seizures were the most difficult to control, has the highest cognitive functioning and has mild ID. The other three siblings have more limited vocabulary and skills, and are functioning in the moderate range of ID. In subject II-4, behavioral problems with aggression towards family and peers are significant and thus she cannot be left alone for any length of time. All have normal strength and can climb, run, and lift objects with no evidence of muscle weakness. None of the sibs has any ophthalmologic concerns.

Common physical features include abnormalities in dentition including enamel hypoplasia, anterior overbite and medial deviation of the mandibular dentition, and flexion contractures of the proximal interphalangeal joints of the 5th fingers (Table 1). Muscle strength and head circumferences are normal. Clinical images of all siblings are shown in the Supplementary Material, Figure S1. Individual II-3, age 23 years, has mild facial dysmorphism with mid-facial hypoplasia, low nasal bridge, several hyperpigmented macules on the tongue, flattening of the helix and bilateral epicanthal folds. She has extensive lymphaedema of both lower extremities and her left upper extremity, which began following a fungal infection 10 years ago. She is also the only sib with borderline growth restriction.

Both parents have university degrees. Family history is negative for any other individuals with seizure disorder or intellectual disability.

Electroencephalogram (EEG) findings: Subject II-2 had an EEG at age 27 years which showed a moderate degree of generalized slowing in the theta range and an epileptic sharp wave in the left temporal region (Fig. 2A and B). EEG for the other three siblings was not possible, due to behavioral issues. These siblings had EEGs which were reportedly normal in childhood, but details were not available. Sleep EEG's and video-EEG telemetry could not be carried out due to practical considerations.

Diagnostic imaging: MRI of the head in subject II-1, II-2, and II-3 showed bilateral periventricular heterotopias in the temporal lobes (Fig. 2C–E). Subject II-2 also showed a probable developmental venous anomaly in the superior temporal gyrus white matter and subject II-3 showed a stable downward displacement of the cerebellar tonsils, consistent with Arnold-Chiari type I malformation (Table 1). MRI scans at 1.5 T MR scanner in subject II-4 were normal with no definite evidence of neuronal migration defects.

Compound heterozygous *TMTC3* variants in patients with nocturnal seizures and ID

Based on the family pedigree (Fig. 1A), dominant as well as recessive disease models were applied to determine the genetic

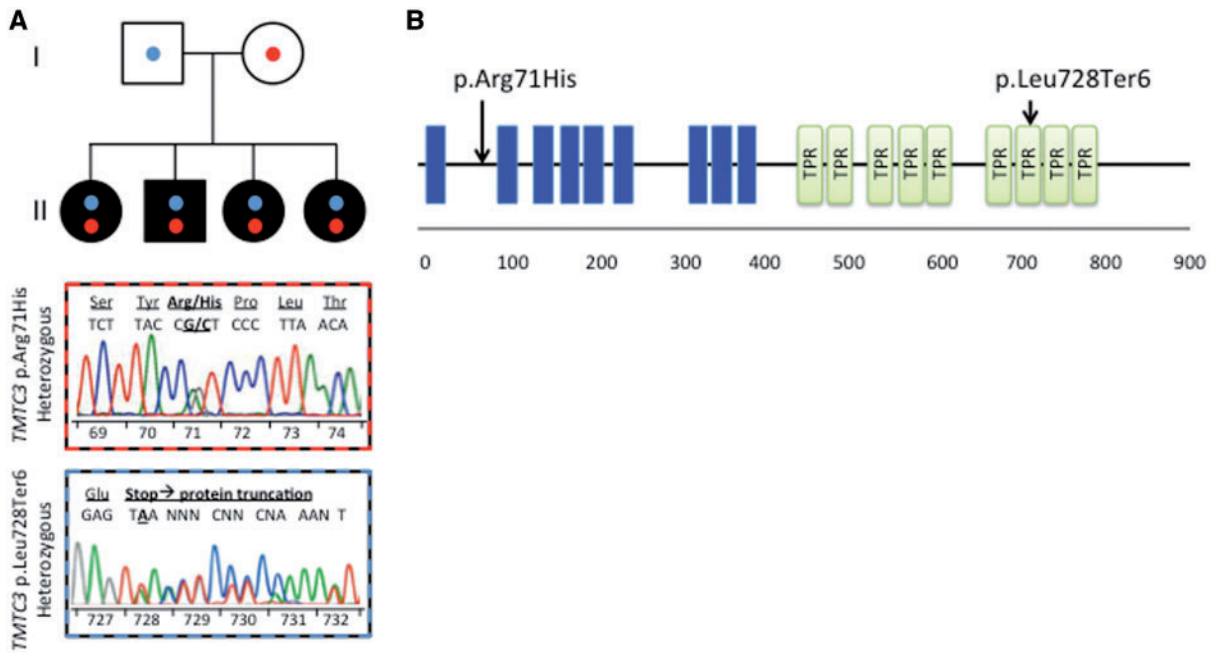

Figure 1. Compound heterozygous *TMTC3* variants in patients with nocturnal seizures with developmental delay. (**A**) Pedigree and electropherograms of the compound heterozygous *TMTC3* variants in patients with nocturnal seizures with intellectual disability. Different colored circles in pedigrees represent different variants. (**B**) Protein structure and associated domains of TMTC3 with respective variants identified. RefSeq numbers: NM_181783.3 and NP_ 861448.2. Transmembrane regions are shown in blue and the tetratricopeptide repeats (TPR) domains are shown in green. The location of the TMTC3 variants is shown with the black arrows.

Table 1. Clinical features of patients with nocturnal seizures with ID

Affected individuals				
Clinical Features	II-1	II-2	II-3	II-4
Gestation	41 weeks	41 weeks	41 weeks	40 weeks
Delivery complications	Induced	None	Breech, caesarean section	Repeat caesarean section
Sex	F	M	F	F
Karyotype	46, XX	46, XY	46, XX	46, XX
Birth weight (g)	4, 082(+2 SD)	3, 401(0 SD)	3, 855 (+1 SD)	3, 402 (0 SD)
Age at last assessment (years)	30	28	23	21
Head circumference (cm)	53.5 (-1SD)	55.8 (+1 SD)	53.7 (−1 SD)	53.3 (−1 SD)
Height (cm)	164 (+1 SD)	168 (−1 SD)	150 (−2 SD)	159.5 (0 SD)
Weight (kg)	54.4 (−0.5 SD)	66.5 (+0.2 SD)	46.2 (−2 SD)	64.8 (+1 SD)
Associated diagnoses				
Age to walk	9 months	< 1 year	< 1 year	< 1 year
Age to talk	1 year	< 1 year	4 years	< 1 year
Able to read	+	+	−	−
Age at onset of nocturnal seizures (years)	2	5	3	3
Enamel hypoplasia	+	−	+	+
Palate	N	N	High arched	N
Anterior overbite	+	−	+	+
Medial deviation of mandibular dentition	+	−	−	+
Tongue hyperpigmentation	+, single location	−	+, extensive	−
Flexion contracture of 5th PIP	+	−	+	+
Hair follicle hyperpigmentation	−	+	+	−
Lymphaedema	−	−	+	−
Hyperactive deep tendon reflexes	+	+	+	+
Hallux valgus	+	+	+	+
MRI findings				
Cobblestone lissencephaly	−	−	−	−
Bilateral periventricular heterotopias	+	+	+	−
Chiari I malformation	−	−	+	−
Venous anomaly	−	+	−	−

Abbreviations: N, normal; +, present; −, absent; MRI, magnetic resonance imaging.

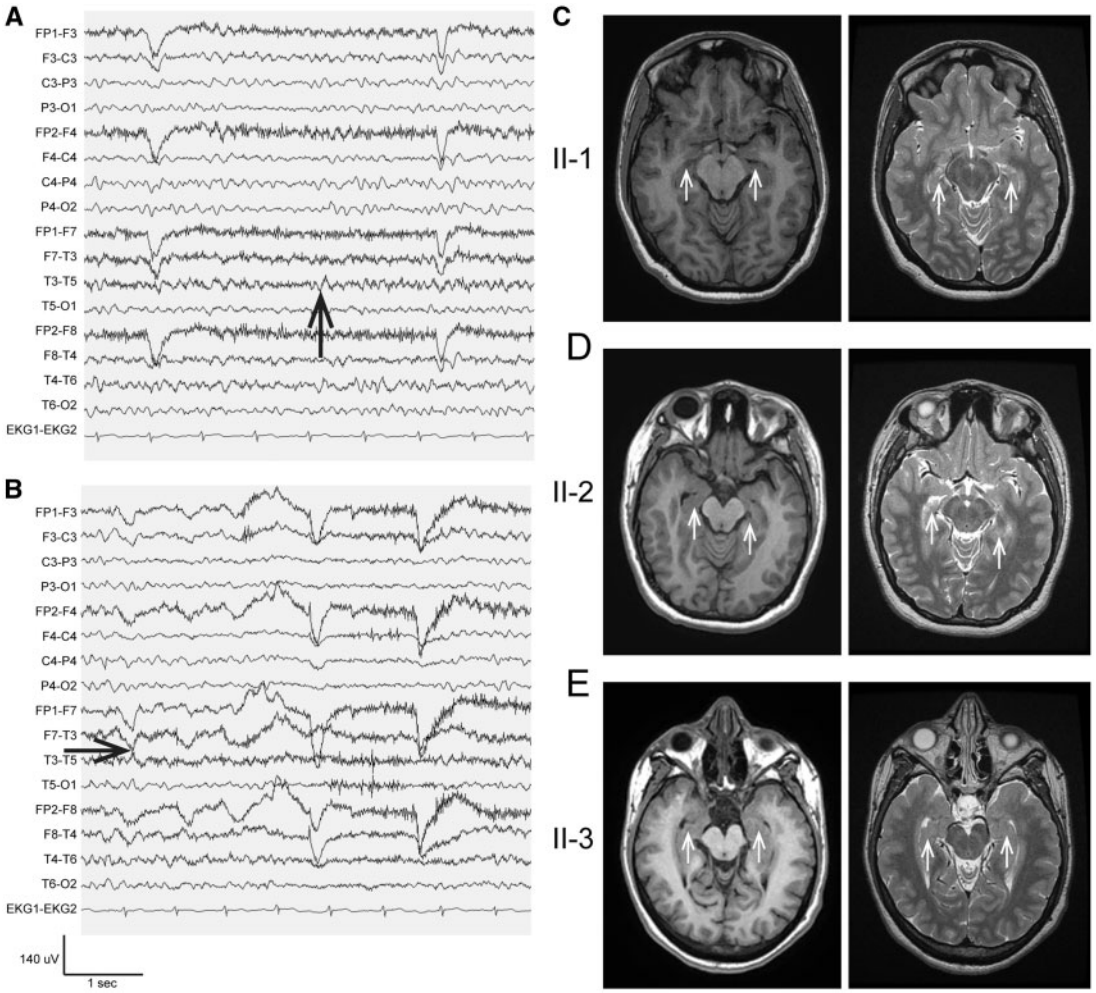

Figure 2. EEG and MRI findings. (**A,B**) Routine scalp EEG recording from subject II-2 at age 26 years: (A) Interictal recording showing diffuse slowing that is most pronounced in the bitemporal regions (maximum left, arrow). (B) Same recording that also displays an epileptic sharp wave in the left temporal region (arrow). Bipolar recording, sensitivity 7 μV/mm, and bandpass filtered between 0.1 Hz and 70 Hz without a notch filter. The extended standard International 10–20 system of electrode placements was used. EEG for subjects II-1, II-3, and II-4 was not possible, due to behavioral issues. (**C,D**) Cranial MRI studies: Axial T1-weighted (left panels) and axial T2-weighted (right panels) fast spin-echo images of subjects II-1 (**C**), II-2 (D), II-3 (**E**) show bilateral periventricular heterotopias around the temporal horns (arrows). Subject II-4 showed no visible abnormalities.

cause of the disease. Through whole exome sequencing, we observed two novel compound heterozygous variants (c.432 G > C, p.Arg71His; and c.2404insA, p.Leu728fsTer6) in *TMTC3* in the affected individuals (Fig. 1B). *TMTC3* encodes the transmembrane and tetratricopeptide repeat containing 3 protein. These variants have not been reported in the Exome Aggregation Consortium (ExAC) database. Overall, there are no homozygous *TMTC3* protein truncating variants found in ExAC, which further supports candidate pathogenicity of these variants.

TMTC3 contains 914 amino acids and is characterized by 9 transmembrane domains and 9 tetratricopeptide repeat (TPR) domains (Fig. 1B). Although the p.Arg71His variant is not located within any of these functional domains, multiple *in silico* analyses predicted the variant to be detrimental to protein function. This amino acid is conserved in mammals, zebrafish, and *Drosophila*, suggesting an important role in the function of the protein. The p.Leu728fsTer6 variant is predicted to cause truncation of the protein leading to complete loss of the final three TPR domains (Fig. 1B). TPR domains are critical for protein interactions and are known to be functional only in groups of 3 or 4. These domains represent the main functional component of TMTC3, and therefore their loss is likely to have a drastic impact on the protein. Furthermore, both *TMTC3* variants segregated with disease status in the family (Fig. 1A). All four children are heterozygous for both variants, whereas the father is heterozygous only for p.Leu728fsTer6 and the mother is heterozygous only for p.Arg71His.

Loss of TMTC3 in patients with nocturnal seizures and ID

To determine the effect of the *TMTC3* variants on protein and transcript expression, we evaluated TMTC3 expression levels via immunoblotting and RT-PCR, respectively, using patient derived fibroblast cells. We observed complete loss of TMTC3 protein in fibroblast cells extracted from two affected individuals relative to both parents and a healthy TMTC3 wild type control

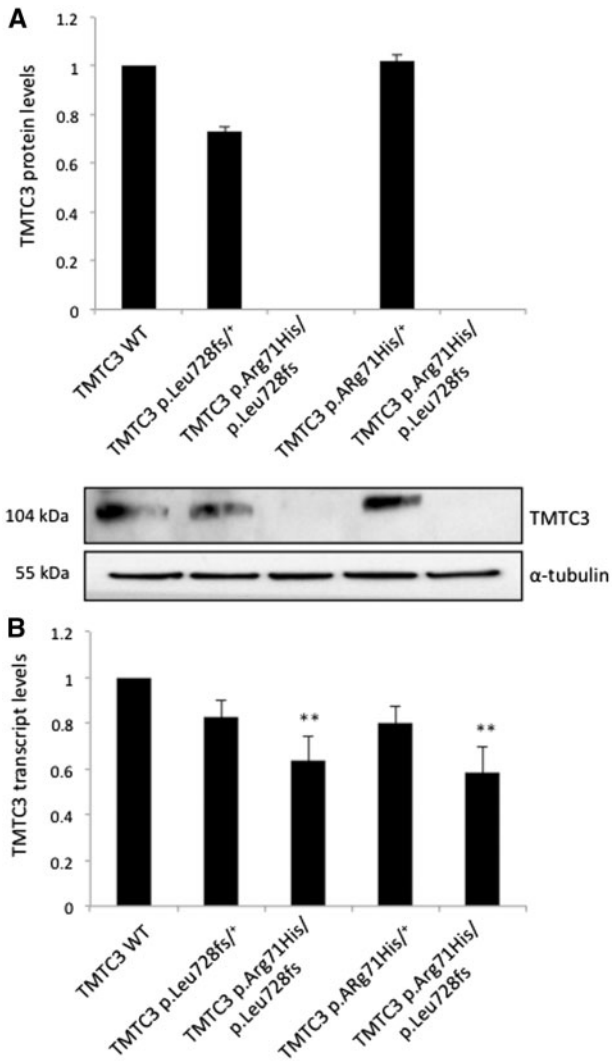

Figure 3. Depleted TMTC3 protein and transcript expression in cells of patients affected by nocturnal seizures with developmental delay. (**A**) Immunoblotting analysis showing depleted TMTC3 protein expression in fibroblast cells of patients with nocturnal seizures with intellectual disability. The upper blot shows protein expression of TMTC3, relative to TMTC3 wild type (WT), TMTC3 p.Arg71His/+ (parent 1), and TMTC3 p.Leu728fsTer6/+ (parent 2). The lower blot shows the constitutive expression of α-tubulin as a loading control. Error bars represent standard error of the mean. The data are representative of four separate, independent experiments. The Student's *t*-test was used to determine the significance of the differences. (**B**) RT-PCR show TMTC3 transcript expression in patients, both parents, and a healthy control. The data are representative of six independent biological replicates. The Student's *t*-test was used to determine the significance of the differences. A *P*-value of less than 0.05 was considered significant. Bar graphs indicate means ± standard deviations. ** represents *P*-value <0.01.

(Fig. 3A). *TMTC3* transcript expression was detected in patient cells but at significantly lower levels than both in parents and a control ($P < 0.01$) (Fig. 3B). Since the TMTC3 antibody used here is directed against the C-terminal of the protein, we cannot rule out the production of a truncated protein product from the p.Leu728fsTer6 allele, however, our data demonstrate that any protein product from the p.Arg71His missense mutation is degraded. These findings suggest that the observed TMTC3 mutations likely underlie nocturnal seizures and ID.

Neuronal knockdown of *Drosophila* tmtc3 causes increased susceptibility to mechanically induced seizures

Having identified *TMTC3* loss of function mutations in four sibling presenting with epilepsy, we sought to investigate the role of TMTC3 in seizure biology. The TMTC3 protein is highly conserved (60% amino acid similarity and 46% identity) and displays a one-to-one orthology with the *Drosophila* protein encoded by *CG4050*, here referred to as *tmtc3*. According to large scale expression data available on FlyBase, *Drosophila tmtc3* is widely expressed, including a relatively high expression level in the adult brain and larval central nervous system (8). Over the course of development, however, *tmtc3* has it highest expression in the early embryo (9). Because of the broad expression pattern, and the high expression in early development, we sought to analyze adult flies with a neuron specific *TMTC3* knockdown rather than germline mutants, which may have phenotypes related to non-neuronal tissue or early developmental defects. To this end, we tested two Gal4-responsive RNAi transgenes encoding inverted repeats (IR) homologous to *Drosophila tmtc3*, *UAS-tmtc3-IR1* and *UAS-tmtc3-IR2*. When RNAi expression was induced using the ubiquitous actin promoter to drive Gal4 expression there was a 70% reduction in *tmtc3* mRNA with *UAS-tmtc3-IR1* and only a 20% reduction with *UAS-tmtc3-IR2* (Fig. 4A), therefore our analysis focuses on *UAS-tmtc3-IR1*.

We investigated the function of *tmtc3* in flies using an established seizure paradigm known as bang sensitivity (10,11). In this assay, seizure-like behaviors are induced by mechanical disturbance (vortexing). The response is measured as the amount of time that individual flies are immobilized on their back and unable to right themselves onto their feet. To test for a role in mechanically induced seizures, we used flies with a neuron-specific RNAi knockdown of *tmtc3* (genotype: *elav-Gal4/+; UAS-dcr2/UAS-tmtc3-IR1*) and compared these to genetic background controls possessing the *elav-Gal4* driver with no RNAi, or the *tmtc3* RNAi transgene with no Gal4 driver (genotypes: *elav-Gal4/+; UAS-dcr2/+* and *+/+; UAS-tmtc3-IR1/UAS-dcr2*). Notably, the proportion of flies experiencing immobilization in response to vortexing was increased by more than 2-fold upon neuron specific knockdown of *tmtc3* compared to both controls (Fig. 4B; see Supplementary videos showing: a normal response with no immobilization in Supplementary Video S1; and a seizure-like response demonstrating immobilization on the back and uncontrollable movement in Supplementary Video S2). To confirm the specificity of this RNAi induced phenotype, we performed rescue experiments using two independent human *TMTC3* transgenes (rescue genotypes: *elav-Gal4/UAS-hTMTC3-1; UAS-dcr2/UAS-tmtc3-IR1* and *elav-Gal4/UAS-hTMTC3-2; UAS-dcr2/UAS-tmtc3-IR1*). Expression of both human transgenes did cause a significant reduction in the proportion of flies immobilized in response to vortexing, when compared to knockdown flies (Fig. 4B). Finally, we tested an additional genotype that expresses a *UAS-GFP* transgene in in place of the human *UAS-hTMTC3* transgenes (genotypes: *elav-Gal4/UAS-GFP; UAS-dcr2/UAS-tmtc3-IR1*). The purpose of this control is to ensure that the observed rescue by the human *TMTC3* transgene is not due to the addition of an extra UAS site, which may titrate the available Gal4 protein such that the RNAi expression becomes too low to efficiently induce a knockdown. The presence of an additional UAS site did not significantly reduce the proportion of immobilized flies compared to UAS-tmtc3-IR1 alone ($P = 0.21$). The proportion of flies immobilized in the presence of UAS-GFP was clearly greater than that of the controls and the human

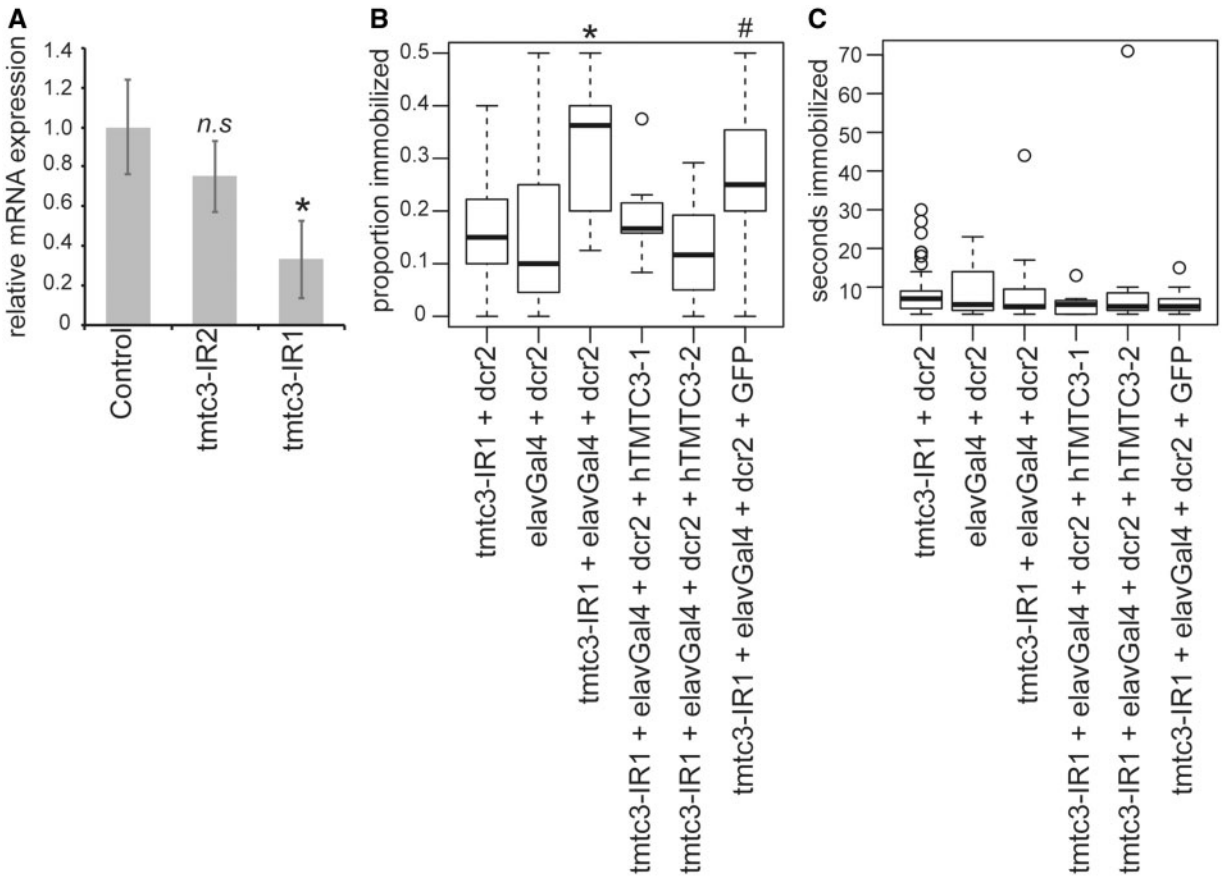

Figure 4. Neuron-specific knockdown of *Drosophila* tmtc3 causes increased susceptibility to mechanically induced seizures. (**A**) qPCR results showing average tmtc3 expression levels (±SEM) in whole larvae with ubiquitous *UAS-tmtc3-IR* expression compared to controls. Significant reduction in tmtc3 mRNA ($P < 0.05$, Students *t*-test) was observed with IR1 but not IR2. (**B**) Boxplot showing the proportion of flies that are immobilized in response to vortexing. Genotypes were compared using the Wilcoxon rank test. * - indicates a significant difference with controls (*tmtc3-IR1 + dcr2*, $P = 0.0006$; *elavGal4 + dcr2*, $P = 0.02$) and rescue genotypes (*hTMT3-1*, $P = 0.04$; *hTMTC3-2*, $P = 0.008$). # - indicates a significant difference with *tmtc3-IR1 + dcr2* ($P = 0.004$) and *hTMTC3-2* ($P = 0.02$), and a borderline significant difference with *elavGal4 + dcr2* ($P = 0.06$) and *hTMT3-1* ($P = 0.08$). (**C**) Boxplots showing the righting time of flies that were immobilized in response to vortexing.

transgenic rescue genotypes (Fig. 4B), and this difference was statistically significant or approaching significant (tmtc3-IR1 $P = 0.004$; elavGal4 $P = 0.06$; hTMTC3-1 $P = 0.08$; hTMTC3-2 $P = 0.02$). Therefore, it appears that *tmtc3* knockdown in neurons increases susceptibility to mechanically induced seizure in *Drosophila*, and this phenotype can be recovered by transgenic rescue in a humanized fly.

In addition to seizure susceptibility proportions at the population level, we also examined the duration of immobilization in response to vortexing for each individual fly. When considering only flies that were immobilized, the median recovery time is similar between all genotypes (Fig. 4C), suggesting that *tmtc3* knockdown does not affect seizure severity, but rather increases the probability of immobilization in response to vortexing.

To further elucidate the underlying mechanisms of the observed immobilization phenotype, we investigated whether the knockdown of *Drosophila tmtc3* may cause changes in neuronal morphology. We identified no morphological differences upon examination of several different neuronal structures in *tmtc3* knockdown flies; including gross mushroom body morphology (Supplementary Material, Fig. S2A and B), dendrite arborization in type 4 multidendrite neurons (Supplementary Material, Fig. S2C–E), and synaptic morphology at the neuromuscular junction (Supplementary Material, Fig. S2F–H). These structures represent model systems for the analysis of axon, dendrite, and synaptic morphogenesis, respectively. This suggests that *Drosophila tmtc3* may not have a widespread role in the regulation of neuronal morphogenesis, however, this analysis is limited to post mitotic knockdown and it is possible that germline null mutations may have a different effect.

TMTC3 is localized at presynaptic terminals in rat brains

TMTC3 is a predicted membrane protein containing 9 transmembrane domains, and has been shown to partially co-localize with an endoplasmic reticulum marker in cultured odontoblasts (12). Considering that TMTC3 has a functional role in *Drosophila* neurons and appears to play a conserved role in seizure susceptibility in both flies and humans, we sought to investigate the localization of TMTC3 in the mammalian brain, using rat brain sections. First, we used a commercially available anti-TMTC3 antibody (sc-398137, Santa Cruz) directed against the human protein, which has 90% amino acid identity to rat Tmtc3. This antibody showed a restricted expression of TMTC3 with the only significant signal appearing in the hypothalamus

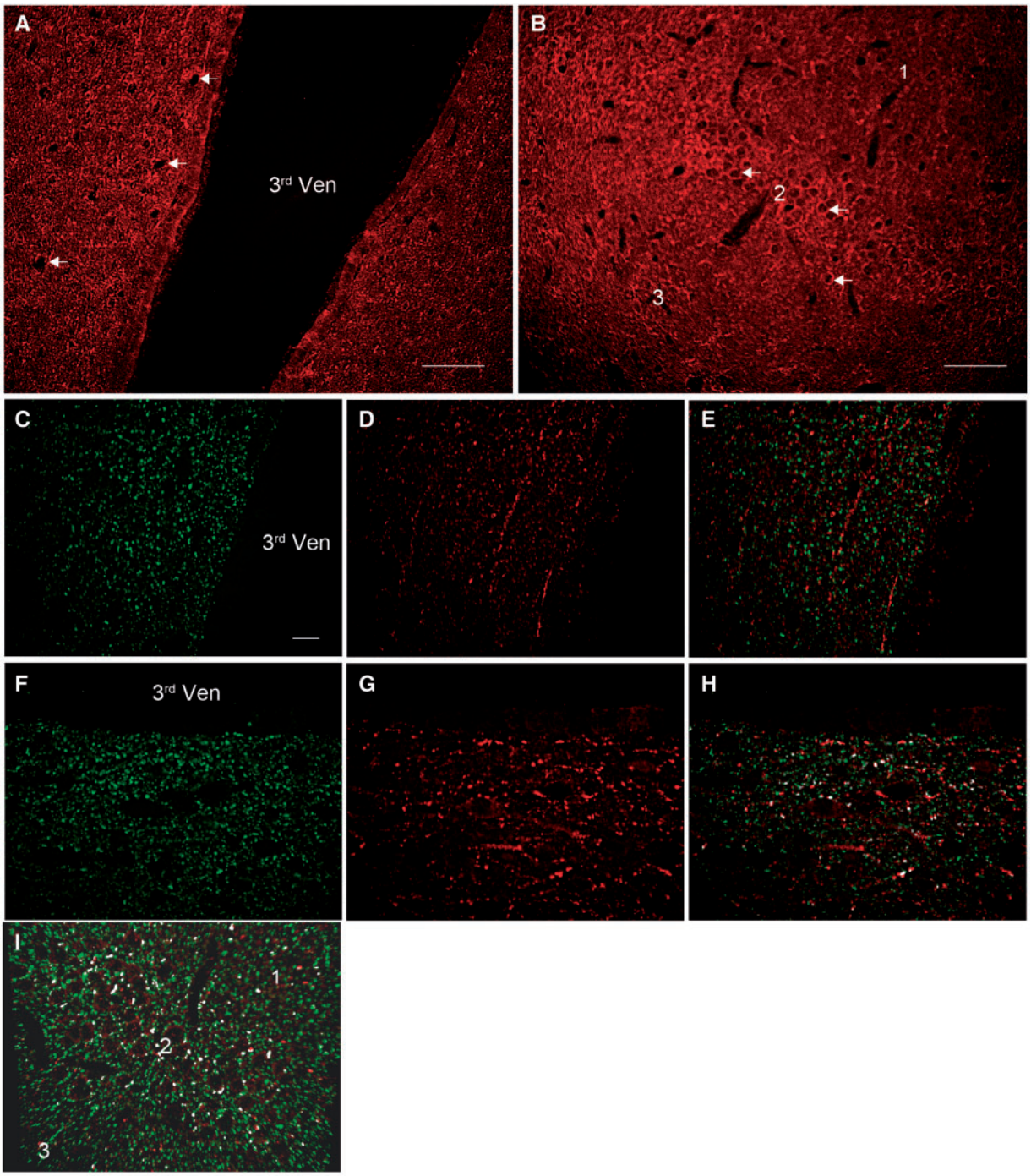

Figure 5. TMTC3 is expressed in hypothalamus and piriform cortex of rat brain and co-localizes with vesicular GABA transporter (VGAT) but not vesicular glutamate transporter 2 (Vglut2). (**A,B**) Low magnification images of TMTC3 immunoreactivity in hypothalamus adjacent to the third ventricle (A) and in piriform cortex (layers 1-3 are indicated) (B). Both images show punta surrounding immunonegative cell bodies; examples of which are marked with white arrows (scale bar is 100 μm). (**C–E**) Confocal images of the rat hypothalamus showing that TMTC3 does not co-localize with Vglut2, a marker of excitatory nerve terminals. (C) shows Vglut2 staining while panel (D) shows TMTC3 expression. (E) is a merged image stack. (**F–H**) VGAT is co-localized with TMTC3 in a subpopulation of VGAT positive puncta in the hypothalamus, along the third ventricle. (F) shows VGAT immunoreactivity while (G) shows TMTC3 immunoreactivity. (H) Merged image showing that TMTC3 and VGAT are co-localized in puncta surrounding cell bodies. White represents voxels, where TMTC3 and VGAT are colocalized in three dimensions (60X mag, scale bar is 20 μm). In (**I**), we show merged channels and co-localization of TMTC3/VGAT at 60 X magnification in piriform cortex. (layers 1–3 are indicated).

and piriform cortex (Fig. 5A and B). Immunoreactivity was observed to be punctate and not localized in cell bodies (see white arrows in A and B). This pattern of expression was completely blocked using a blocking peptide against sc-398173, suggesting that the signal is highly specific.

High magnification (60X) images confirm that TMTC3 immunofluorescence is indeed highly punctate, concentrated around cell bodies, but largely absent within cell bodies. We hypothesized that this expression could be in nerve terminals within these regions. To test this, we performed co-localization

analysis with vesicular GABA transporter (VGAT), a presynaptic marker for inhibitory synapses, and vesicular glutamate transporter 2 (Vglut2), a presynaptic marker for excitatory synapses. TMTC3 did not appreciably co-localize with Vglut2 (Fig. 5C–E). To examine TMTC3 co-localization with VGAT we used a different TMTC3 antibody obtained from another supplier (ab81473; see Methods), as both TMTC3 (sc-398173) and our VGAT antibodies (Synaptic Systems, 131011) were raised in the same species (mouse). As the peptide information for ab81473 is proprietary, we were unable to obtain a blocking peptide to directly demonstrate specificity. However, the second TMTC3 antibody showed an identical pattern of express as the original one, suggesting that ab81473 is specific for TMTC3 (compare Fig. 5D and G). Using this antibody, we found that TMTC3 was colocalized with a subpopulation of VGAT positive puncta in the hypothalamus (Fig. 5F–H) and piriform cortex (Fig. 5I).

These data show that TMTC3 is localized in a subpopulation of GABAergic inhibitory synaptic terminals and boutons, and absent from excitatory glutamatergic presynapses.

Discussion

PVNH is one of the most common forms of cortical brain malformation and for most cases there is no genetic diagnosis. Here, we identify *TMTC3* mutations as a novel cause of PVNH, accompanied by nocturnal epileptic seizures and ID (Figs 1–3, Table 1). The identified *TMTC3* variants have not been reported in any publicly accessible database of genetic variation and our whole exome analysis did not reveal any other plausible candidate genetic variants in the four affected siblings. The ExAC database does not report a single example of homozygous loss of function or damaging missense mutations in *TMTC3*, indicating that disruption of the TMTC3 protein is likely to be detrimental to cell function. The implication of TMTC3 in PVNH is consistent with a recent report by Jerber *et al.*, which identified a role for *TMTC3* in COB, which also results from defects in neuronal migration (13). COB represents over-migration of neuronal cells, whereas PVNH occurs when neurons fail to migrate from the ventricles. Jerber *et al.*, studied 25 families with COB, and six families (nine patients) carried recessive variants in *TMTC3*, none of whom carried the same recessive variants as the patients described herein. Frameshift or nonsense variants were found in 8 of 14 alleles, and 4 out of 6 families. All nine patients had ID, delayed gross and fine motor skills, delayed language development, and defects in neuronal migration. Eight of nine patients had the hallmark clinical feature, COB, while the remaining individual had subcortical and periventricular hypomyelination, which has been described to precede patchy dysmyelination, and overmigration of neuronal cells in the leptomeningeal space. The majority of patients (six of nine) had diurnal seizures commencing between 4 and 8 months. These observations, in combination with our study, collectively support a role for *TMTC3* in a spectrum of cortical malformation disorders causing ID and epilepsy. Our study highlights the clinical variability that can be associated with *TMTC3* mutations, by identification of individuals with clear loss of TMTC3 function, who present with a milder phenotype of nocturnal seizures and PVNH.

Functionally, we demonstrate a neuron-specific role for *TMTC3* in *Drosophila* seizure susceptibility (Fig. 4). The "bang sensitivity" test employed here is a classic assay for mechanically induced seizure, characterized by immobilization in response to a strong mechanical stimulus (14). Loss of *Drosophila tmtc3* specifically in post-mitotic neurons doubles the rate of immobilization in response to vortexing (Fig. 4B), suggesting that loss of *tmtc3* renders neurons susceptible to seizure. This phenotype is rescued by expression of a human *TMTC3* transgene specifically in neurons. Therefore, although the seizure paradigm employed here is not directly comparable to the human condition, we have illustrated that the human protein is functionally relevant in the context of mechanically induced seizures in *Drosophila*. To date, this type of humanized rescue experiment is not standard in *Drosophila* studies investigating human disease genes. However, recent studies have shown that this can be an effective means of assessing human gene function, and potentially disease causing mutations in flies (15–20).

The suspected mechanisms underlying cortical malformation disorders associated with epilepsy are primarily related to defects in cytoskeletal organization and cell signaling pathways, such as the Akt-mTOR pathway. Recently, NEDD4L was associated with PVNH and dysregulation of mTor signaling (21). Other components of the mTor signaling pathway, including the GATOR1 complex and TSC1/2, have been implicated in epilepsy with focal cortical dysplasia and diverse brain lesions suggestive of global defects in neuronal migration (22,23). The potential link between TMTC3 and these biological processes remains unclear.

TMTC3 is a membrane protein that contains several TPR-domains, which mediate protein-protein interactions in many different biological processes (24). Here, we show that TMTC3 is localized at inhibitory GABAergic synapses in the hypothalamus and piriform cortex of the rat brain, but is not present at excitatory glutamatergic synapses (Fig. 5). Interestingly, the TMTC3 paralogs, TMTC1 and TMTC2, are predicted to act as adaptors that nucleate the formation of large protein complexes involved in the regulation of calcium transport across the ER membrane (25). Based on the similar domain structure seen in TMTC3, it is possible that this protein plays a similar role at the synapse. This is supported by protein interaction data for TMTC3 from several proteomic studies (26–29), which are annotated through the BioGRID database (30). Of the 21 TMTC3 interactors listed in BioGRID, six are involved in gated ion channel activity (CHRND, HTR3C, HTR3A, ZACN, GABRE, and SCN3B) and five are localized at the synapse (CHRND, HTR3A, NRG1, GABRE, and DAB1; annotations from PANTHER) (31). Interestingly, neuronal migration is known to depend on synaptic activity and the regulation of calcium gradients (32,33). In mice, migration of neurons in the subventricular zone is dependent on tight regulation of GABA release and uptake (34). TMTC3 might regulate neuronal migration through modulation of synaptic activity or through calcium transport at GABAergic synaptic terminals, however, further studies are needed to investigate this possibility.

This study identifies TMTC3 as a novel synaptic protein involved in PVNH, epilepsy and ID, and lays the foundation for future investigations towards understanding the specific role of TMTC3 in the regulation of synaptic function and neuronal migration.

Materials and Methods

Patients

Four children of a healthy non-consanguineous Pakistani couple were diagnosed with nocturnal seizures of unknown cause with ID. Blood and tissue (skin-derived fibroblasts) samples were collected from all four affected children and both parents following appropriate and informed consent in accordance with

the Research Ethics Board at Western University, London, Ontario, Canada.

DNA isolation

DNA was isolated from blood or cultured cells collected from every family member using the Gentra Puregene Blood kit (Qiagen) per the manufacturer's instructions.

Next generation sequencing

Whole exome sequencing was performed using genomic DNA from two affected individuals (II-2 and II-3) on the Illumina HiSeq 2000 with 2x100 paired end chemistry in accordance with library protocols used at The Centre for Applied Genomics (TCAG) at The Hospital for Sick Children, Toronto, Ontario as previously described (35,36). Genome Analysis Toolkit (GATK) was used to generate the coverage of the whole exome in the form of variant calling format (VCF) files as previously described (35,37,38).

Variant discovery

Initially, we applied a dominant model analysis on the patients' exomes with no mutations observed in known epilepsy genes as we were considering the possibility of incomplete penetrance or mosaicism. We also did not observe any promising dominant variants in other genes. We then applied a recessive model of inheritance (homozygous and compound heterozygous) on all variants. We scanned for variants in genes known to cause seizures and/or ID based on literature and OMIM, as well as all protein-coding genes covered by whole exome sequencing. Given the rarity of the disease, we screened for rare variants (minor allele frequency [MAF, <1%]) according to NCBI dbSNP, 1000 Genomes (39), NHLBI ESP Exome Variant Server (40), and Exome Aggregation Consortium (ExAC) (41) datasets to identify any variants. To determine the predicted biological effect of non-synonymous variants on protein function, candidate variants (p.Arg71His and p.Leu728fsTer6) were assessed using the following predictive *in silico* tools: Polymorphism Phenotyping version 2 (PolyPhen-2) (42), Sorting Intolerant From Tolerant (SIFT) (43), and MutationTaster2 (44). To determine amino acid conservation, human protein sequences were aligned to other protein sequences from a diverged set of species using ClustalW2.

Variant validation

Candidate variants were confirmed by Sanger sequencing, as previously described (35). Forward and reverse primers specific to amplify *TMTC3* (RefSeq number NM_181783.3) g.88153313 on chromosome 12 (p.Arg71His, c.212 G > A) were: 5'-CAGTG ATGAGCTTTTGTACCC-3' and 5'-CACACTACTCTTGTTGTCC-3', respectively; and *TMTC3* g.88195088dupA (p.Leu728fsTer6, c.2184dupA) were: 5'-AAGCCGACTTCCGAAGTGCT-3' and 5'- TT CCTTGCACATTGCTTGG-3'. Primers were designed using GRCh38/hg38. The PCR annealing temperature was 58°C.

Tissue culture

Skin fibroblasts from patients, both parents, and a healthy (*TMTC3* wild type) control were cultured in Petri plates with Dulbecco's modified Eagle's medium (GIBCO, Carlsbad, CA, USA) as previously described (35).

Immunoblotting

Protein expression was analyzed by immunoblotting and quantified by densitometry as previously described (35). Anti-TMTC3 (1: 100, Santa Cruz Biotechnology, Dallas, Texas) was used as a primary antibody. For a positive control, α-tubulin (1: 10,000, Sigma-Aldrich, Saint Louis, Missouri) was used. Anti-mouse (1: 10,000, Jackson ImmunoResearch Laboratories, Inc) was used as a secondary antibody.

Reverse transcriptase PCR

RNA was isolated from fibroblast cells using the RNeasy Mini Kit per the manufacturer's instructions (Qiagen) as previously described (35). The data are representative of six independent biological replicates.

Drosophila stocks

Fly lines expressing transgenic RNAi encoding inverted repeats for the *CG4050* gene (33248 and 110199, here referred to as UAS-*tmtc3*-IR1 and UAS-*tmtc3*-IR2, respectively) and the appropriate genetic background control lines (60,000 and 60,100, respectively) were obtained from the Vienna Drosophila Resource Center (Vienna, Austria). *elav-Gal4; UAS-dcr2* was a gift from A. Schenck. *UAS-dcr2* (24644 and 24650), *R14H06-Gal4* (48667) *UAS-mcD8:: GFP* (5130) and *477-Gal4, UAS-mcD8:: GFP* (8746) were obtained from the Bloomington Drosophila Stock Center (Indiana, USA). For creation of transgenic flies with inducible expression of human TMTC3 (*UAS-hTMTC3-1* and *UAS-hTMTC3-2*), *TMTC3* cDNA (Internal ID 53914 of the hORFeome V5.1 of the CCSB Human Orfeome Collection and Entrez Gene ID 160418) was inserted into the pTW vector at the SPARC BioCentre (SickKids Hospital, Toronto) using standard Gateway cloning. Transgenic flies were created using standard P-element based transgenesis at Best Gene Inc. (California, USA).

RT-qPCR

Quantitative Real-Time PCR (RT-qPCR) was performed to evaluate the potency of *UAS-tmtc3-IR1* and *UAS-tmtc3-IR2*. RNAi lines and controls were crossed the ubiquitous *Actin-Gal4* driver line and third instar larvae were selected for analysis. RNA was extracted using the RNeasy Lipid Tissue Mini Kit (Qiagen). cDNA was made using the iScript cDNA synthesis kit (BioRad). RT-qPCR was performed using the BioRad CFX 384 and the SYBRgreen master mix (BioRad) with primers directed against *CG4050*, and the reference genes, *βCOP*, *eIF2Bβ*, and *RpII140*. *CG4050* expression was compared in control and RNAi genotypes using a Student's *t*-test.

Bang sensitivity assays

Bang sensitivity assays were performed using 5–9-day old male flies, raised at 29°C. The following genotypes were analyzed: *UAS-dcr2/+; UAS-tmtc3-IR1/+* ($n = 436$), *elavGal4/+; UAS-dcr2/+* ($n = 69$), *elavGal4/+; UAS-dcr2/UAS-tmtc3-IR1* ($n = 75$), *elavGal4/UAS-hTMTC3-1*; *UAS-dcr2/UAS-tmtc3-IR1* ($n = 54$), *elavGal4/UAS-hTMTC3-2; UAS-dcr2/UAS-tmtc3-IR1* ($n = 51$), and *elavGal4/UAS-GFP; UAS-dcr2/UAS-tmtc3-IR1* ($n = 127$). Male flies were collected

in groups of ten to twelve and aged for several days. For testing, 5–9-day-old flies were transferred to empty food vials without the use of CO_2. After a 5-min acclimatization period, the vials were vortexed at the highest setting for 20 s. Immediately after vortexing, the behavioral response was video recorded. After an additional 10-min rest period, flies were vortexed again in a second trial. Videos were observed for seizure-like responses, characterized by complete immobilization on the back and/or uncontrollable movement for 3 or more seconds (see Video S1 and Video S2). The time of immobilization was recorded for each individual fly as was the proportion of flies immobilized per test vial. The proportion of immobilized flies was averaged between the two trials for each tube and these values were visualized as a box plot (Fig. 4B). Statistical differences between genotypes were compared using the Wilcoxon rank test.

Immunohistochemistry, image acquisition, and analysis

Rat brains: sections were washed with 1x PBS with 0.2% Triton X-100 three times for 5 min and blocked in 10% goat serum and 10% donkey serum in 1x PBS with 0.025% Triton X-100 and 1% bovine serum albumin (BSA) for 1 h. The primary antibodies were diluted in 1x PBS with 1% BSA and 0.025% Triton X-100. The sections were incubated with primary antibodies for 24 h at 4 °C; mouse anti-VGAT antibody (1: 200, Synaptic Systems, 131011) with rabbit anti- TMTC3 (1: 500, Abcam ab81473); or rabbit anti-Vglut2 (1: 2000, Synaptic Systems, 135402) with mouse anti-TMTC3 (1: 200 dilution, Santa Cruz, sc-398137). For blocking with of the sc-398137 antibody, a commercially available peptide was used (Santa Cruz, sc-398137 P). The primary antibody was incubated with the blocking peptide at 1 μg/ml for 30 min before incubation with sections for 24 h at 4 °C. Sections were then washed two times with 1x PBS with 0.2% Triton X-100 for 5 min. They were incubated with secondary antibodies for 1 h at room temperature; Alexa Fluor 647 donkey anti-rabbit IgG (A31573) and Alexa Fluor 488 donkey anti-mouse IgG antibody (Molecular Probes, A-21202) diluted 1: 1000 in PBS with 1% BSA and 0.025% Triton X-100.

Confocal images were taken on an Olympus IX 60 inverted microscope outfitted with a Perkin Elmer spinning disk confocal attachment with either a 60 × (Numerical aperture = 1.4) immersion oil, or 20 × (N.A. = 0.5), objective. The microscope was equipped with a Hamamatsu Orca ER CCD camera (1300 × 1030 pixels; pixel size 6.5 μm) and images were acquired using Volocity software. Each image shown represents a stack of 10 images spaced 0.2 μm apart in the z-plane, for each wavelength. Image stacks were deconvoluted using Autoquant (Media Cybernetics, Bethesda, MD, U.S.A.) software (using the manufacturer supplied PSF adapted for spinning disk microscopy). Analysis of the stacks was performed using IMARIS (Bitplane, Zurich CH) as previously described (45). Briefly, the deconvoluted image stacks were segmented so only the brightest pixels (top 5%) were co-localized with the brightest 5% on the other channel. This generated a third channel shown in white in Figure 5. Image stacks were collapsed to a 2-D image where co-localized volumes (voxels) are shown in white.

Fly multidendritic neurons: The following genotypes were dissected as third instar larvae and fixed in 4% paraformaldehyde: *477-Gal4, UAS-mcD8::GFP/+* (control) and *+/+; 477-Gal4, UAS-mcD8::GFP/UAS-tmtc3-IR1*. Tissue was incubated in PBT (PBS with 0.3% triton-X 100) for 40 min and blocked in PBT supplemented with 5% normal goat serum. Larvae were incubated for two nights with anti-GFP (1: 25, mouse, developmental studies hybridoma bank [DSHB]) and anti-mCD8 (1: 100, rat, Life Technologies) primary antibodies diluted in PBT with 5% NGS. After washing in PBT, larvae were incubated overnight with secondary antibodies anti-mouse-DyLight488 (1: 400, goat, ThermoFisher) and anti-rat-DyLight488 (1: 400, goat, ThermoFisher). Dorsal type IV multidendritic neurons were imaged using a Zeiss LSM 510 DUO Vario confocal microscope. The entire neuron was captured by combining several fields of view using the tile scan function. Image stacks were imported to Neuron Studio and traced (46). Centrifugal edge labeling was performed and analyzed using the LMeasure program to quantify various features of the neurons (47). A student's *t*-test was used to determine if any significant differences were present between the number of bifurcations, number of branches, number of tips, and overall length of the control and *UAS-tmtc3-IR1* Type IV multidendritic neurons.

Fly neuromuscular junction (NMJ): the genotypes *elavGal4/+; UAS-dcr2/+* (control) and *elavGal4/+; UASdcr2/UAS-tmtc3-IR1*, were processed as described above, with the following changes. Primary antibodies used were: anti-HRP (1: 500, rabbit, Jackson Immuno Research) and anti-brp (nc82, 1: 15, mouse, DSHB). Secondary antibodies used were anti-rabbit-DyLight488 (1: 400, goat, ThermoFisher) and anti-mouse-DyLight594 (1: 400, goat, ThermoFisher). To determine whether the knockdown of the *tmtc3* gene had any effect on the morphology of the *Drosophila* NMJ, images of the NMJ were loaded into the open-source image analysis software, Fiji (48). Using the algorithm, 'Drosophila_NMJ_Morphometrics' (49) features of the NMJ were quantified for analysis. A Mann-Whitney test for non-parametric data was used to determine if any significant differences were present between the number of branches, active zones, and the overall length and area of the control and *UAS-tmtc3-IR1* NMJ.

Fly mushroom bodies: The mushroom body specific *R14H06-Gal4* driver line (50) was used to express *tmtc3* RNAi constructs and GFP. Adult male fly brains were dissected from the genotypes *UAS-dcr2/mcD8:: GFP; R14H06-Gal4/UAS-tmtc3-IR1*, and *UAS-dcr2/mcD8GFP; R14H06-Gal4/+*, and fixed for 1 h in 4% paraformaldehyde. GFP labeled mushroom bodies were imaged using a Zeiss LSM 510 DUO Vario confocal microscope.

Supplementary Material

Supplementary Material is available at *HMG* online.

Acknowledgements

We thank and acknowledge the consent and cooperation of the family members. Many thanks to the FORGE Canada Steering Committee: Kym Boycott (leader; University of Ottawa), Jan Friedman (co-lead; University of British Columbia), Jacques Michaud (co-lead; Université de Montréal), Francois Bernier (University of Calgary), Michael Brudno (University of Toronto), Bridget Fernandez (Memorial University), Bartha Knoppers (McGill University), Mark Samuels (Université de Montréal), Steve Scherer (University of Toronto). We would like to thank Janet Marcadier (Clinical Coordinator) and Chandree Beaulieu (Project Manager) for their contribution to the infrastructure of the FORGE Canada Consortium. Many thanks to Jacek Majewski (McGill University) for providing valuable feedback during analyses. Thanks to the Bloomington *Drosophila* Stock Center

(Indiana University), the *Drosophila* Genomics Resource Center (Indiana University), the Vienna *Drosophila* Resource Center (Vienna, Austria), and Annette Schenck (Radboud University Medical Center) for providing *Drosophila* stocks and reagents.

Conflict of Interest statement. None declared.

Funding

This work was supported by the Canadian Rare Disease Models and Mechanisms Network, the Canadian Institute of Health Research (CIHR), and Finding of Rare Disease Genes (FORGE) Canada. FORGE Canada was funded by Genome Canada, CIHR, the Ontario Genomics Institute (OGI-049), Genome Quebec, Genome British Columbia, and the McLaughlin Centre. KCJN is supported by a Queen Elizabeth II Ontario Graduate Scholarship. SMKF is supported by the Canadian Institutes of Health Research Frederick Banting and Charles Best Canada Graduate Scholarship. Funding to pay the Open Access publication charges for this article was provided by the Canada Research Chairs program.

References

1. Liu, J.S. (2011) Molecular genetics of neuronal migration disorders. *Curr. Neurol. Neurosci. Rep.*, **11**, 171–178.
2. Liu, W., Yan, B., An, D., Xiao, J., Hu, F. and Zhou, D. (2017) Sporadic periventricular nodular heterotopia: Classification, phenotype and correlation with Filamin A mutations. *Epilepsy Res.*, **133**, 33–40.
3. Fox, J.W., Lamperti, E.D., Ekşioğlu, Y.Z., Hong, S.E., Feng, Y., Graham, D.A., Scheffer, I.E., Dobyns, W.B., Hirsch, B.A., Radtke, R.A. *et al.* (1998) Mutations in filamin 1 prevent migration of cerebral cortical neurons in human periventricular heterotopia. *Neuron*, **21**, 1315–1325.
4. Sheen, V.L., Ganesh, V.S., Topcu, M., Sebire, G., Bodell, A., Hill, R.S., Grant, P.E., Shugart, Y.Y., Imitola, J., Khoury, S.J. *et al.* (2004) Mutations in ARFGEF2 implicate vesicle trafficking in neural progenitor proliferation and migration in the human cerebral cortex. *Nat. Genet.*, **36**, 69–76.
5. Conti, V., Carabalona, A., Pallesi-Pocachard, E., Parrini, E., Leventer, R.J., Buhler, E., McGillivray, G., Michel, F.J., Striano, P., Mei, D. *et al.* (2013) Periventricular heterotopia in 6q terminal deletion syndrome: role of the C6orf70 gene. *Brain*, **136**, 3378–3394.
6. Broix, L., Jagline, H., L Ivanova, E., Schmucker, S., Drouot, N., Clayton-Smith, J., Pagnamenta, A.T., Metcalfe, K.A., Isidor, B., Louvier, U.W. *et al.* (2016) Mutations in the HECT domain of NEDD4L lead to AKT-mTOR pathway deregulation and cause periventricular nodular heterotopia. *Nat. Genet.*, **48**, 1349–1358.
7. Ferland, R.J., Batiz, L.F., Neal, J., Lian, G., Bundock, E., Lu, J., Hsiao, Y.C., Diamond, R., Mei, D., Banham, A.H. *et al.* (2009) Disruption of neural progenitors along the ventricular and subventricular zones in periventricular heterotopia. *Hum. Mol. Genet.*, **18**, 497–516.
8. Chintapalli, V.R., Wang, J. and Dow, J.A. (2007) Using FlyAtlas to identify better Drosophila melanogaster models of human disease. *Nat. Genet.*, **39**, 715–720.
9. Graveley, B.R., Brooks, A.N., Carlson, J.W., Duff, M.O., Landolin, J.M., Yang, L., Artieri, C.G., van Baren, M.J., Boley, N., Booth, B.W. *et al.* (2011) The developmental transcriptome of Drosophila melanogaster. *Nature*, **471**, 473–479.
10. Ganetzky, B. and Wu, C.F. (1982) Indirect suppression involving behavioral mutants with altered nerve excitability in DROSOPHILA MELANOGASTER. *Genetics*, **100**, 597–614.
11. Howlett, I.C., Rusan, Z.M., Parker, L. and Tanouye, M.A. (2013) Drosophila as a model for intractable epilepsy: gilgamesh suppresses seizures in para(bss1) heterozygote flies. *G3*, **3**, 1399–1407.
12. Racape, M., Duong Van Huyen, J.P., Danger, R., Giral, M., Bleicher, F., Foucher, Y., Pallier, A., Pilet, P., Tafelmeyer, P., Ashton-Chess, J. *et al.* (2011) The involvement of SMILE/TMTC3 in endoplasmic reticulum stress response. *PLoS One*, **6**, e19321.
13. Jerber, J., Zaki, M.S., Al-Aama, J.Y., Rosti, R.O., Ben-Omran, T., Dikoglu, E., Silhavy, J.L., Caglar, C., Musaev, D., Albrecht, B. *et al.* (2016) Biallelic Mutations in TMTC3, Encoding a Transmembrane and TPR-Containing Protein, Lead to Cobblestone Lissencephaly. *Am. J. Hum. Genet.*, **99**, 1181–1189.
14. Song, J. and Tanouye, M.A. (2008) From bench to drug: human seizure modeling using Drosophila. *Prog. Neurobiol.*, **84**, 182–191.
15. Chao, H.T., Davids, M., Burke, E., Pappas, J.G., Rosenfeld, J.A., McCarty, A.J., Davis, T., Wolfe, L., Toro, C., Tifft, C. *et al.* (2017) A syndromic neurodevelopmental disorder caused by de novo variants in EBF3. *Am. J. Hum. Genet.*, **100**, 128–137.
16. Jakobsdottir, J., van der Lee, S.J., Bis, J.C., Chouraki, V., Li-Kroeger, D., Yamamoto, S., Grove, M.L., Naj, A., Vronskaya, M., Salazar, J.L. *et al.* (2016) Rare functional variant in TM2D3 is associated with late-onset Alzheimer's disease. *PLoS Genet.*, **12**, e1006327.
17. Fischer, B., Luthy, K., Paesmans, J., De Koninck, C., Maes, I., Swerts, J., Kuenen, S., Uytterhoeven, V., Verstreken, P. and Versees, W. (2016) Skywalker-TBC1D24 has a lipid-binding pocket mutated in epilepsy and required for synaptic function. *Nat. Struct. Mol. Biol.*, **23**, 965–973.
18. Ehaideb, S.N., Iyengar, A., Ueda, A., Iacobucci, G.J., Cranston, C., Bassuk, A.G., Gubb, D., Axelrod, J.D., Gunawardena, S., Wu, C.F. *et al.* (2014) prickle modulates microtubule polarity and axonal transport to ameliorate seizures in flies. *Proc. Natl Acad. Sci. USA*, **111**, 11187–11192.
19. Paemka, L., Mahajan, V.B., Ehaideb, S.N., Skeie, J.M., Tan, M.C., Wu, S., Cox, A.J., Sowers, L.P., Gecz, J., Jolly, L. *et al.* (2015) Seizures are regulated by ubiquitin-specific peptidase 9 X-linked (USP9X), a de-ubiquitinase. *PLoS Genet.*, **11**, e1005022.
20. Schutte, R.J., Schutte, S.S., Algara, J., Barragan, E.V., Gilligan, J., Staber, C., Savva, Y.A., Smith, M.A., Reenan, R. and O'Dowd, D.K. (2014) Knock-in model of Dravet syndrome reveals a constitutive and conditional reduction in sodium current. *J. Neurophysiol.*, **112**, 903–912.
21. Weckhuysen, S., Marsan, E., Lambrecq, V., Marchal, C., Morin-Brureau, M., An-Gourfinkel, I., Baulac, M., Fohlen, M., Kallay Zetchi, C., Seeck, M. *et al.* (2016) Involvement of GATOR complex genes in familial focal epilepsies and focal cortical dysplasia. *Epilepsia*, **57**, 994–1003.
22. DiMario, F.J. Jr. (2004) Brain abnormalities in tuberous sclerosis complex. *J. Child Neurol.*, **19**, 650–657.
23. Baulac, S., Ishida, S., Marsan, E., Miquel, C., Biraben, A., Nguyen, D.K., Nordli, D., Cossette, P., Nguyen, S., Lambrecq, V. *et al.* (2015) Familial focal epilepsy with focal cortical dysplasia due to DEPDC5 mutations. *Ann. Neurol.*, **77**, 675–683.
24. D'Andrea, L.D. and Regan, L. (2003) TPR proteins: the versatile helix. *Trends Biochem. Sci.*, **28**, 655–662.
25. Sunryd, J.C., Cheon, B., Graham, J.B., Giorda, K.M., Fissore, R.A. and Hebert, D.N. (2014) TMTC1 and TMTC2 are novel endoplasmic reticulum tetratricopeptide repeat-containing

adapter proteins involved in calcium homeostasis. *J. Biol. Chem.*, **289**, 16085–16099.
26. Gupta, G.D., Coyaud, E., Goncalves, J., Mojarad, B.A., Liu, Y., Wu, Q., Gheiratmand, L., Comartin, D., Tkach, J.M., Cheung, S.W. *et al.* (2015) A dynamic protein interaction landscape of the human centrosome-cilium interface. *Cell*, **163**, 1484–1499.
27. Hein, M.Y., Hubner, N.C., Poser, I., Cox, J., Nagaraj, N., Toyoda, Y., Gak, I.A., Weisswange, I., Mansfeld, J., Buchholz, F. *et al.* (2015) A human interactome in three quantitative dimensions organized by stoichiometries and abundances. *Cell*, **163**, 712–723.
28. Huttlin, E.L., Ting, L., Bruckner, R.J., Gebreab, F., Gygi, M.P., Szpyt, J., Tam, S., Zarraga, G., Colby, G., Baltier, K. *et al.* (2015) The BioPlex Network: a systematic exploration of the human interactome. *Cell*, **162**, 425–440.
29. Rolland, T., Taşan, M., Charloteaux, B., Pevzner, S.J., Zhong, Q., Sahni, N., Yi, S., Lemmens, I., Fontanillo, C., Mosca, R. *et al.* (2014) A proteome-scale map of the human interactome network. *Cell*, **159**, 1212–1226.
30. Chatr-Aryamontri, A., Breitkreutz, B.J., Oughtred, R., Boucher, L., Heinicke, S., Chen, D., Stark, C., Breitkreutz, A., Kolas, N., O'Donnell, L. *et al.* (2015) The BioGRID interaction database: 2015 update. *Nucleic Acids Res.*, **43**, D470–D478.
31. Mi, H., Lazareva-Ulitsky, B., Loo, R., Kejariwal, A., Vandergriff, J., Rabkin, S., Guo, N., Muruganujan, A., Doremieux, O., Campbell, M.J. *et al.* (2005) The PANTHER database of protein families, subfamilies, functions and pathways. *Nucleic Acids Res.*, **33**, D284–D288.
32. Spitzer, N.C. (2006) Electrical activity in early neuronal development. *Nature*, **444**, 707–712.
33. Komuro, H. and Rakic, P. (1996) Intracellular Ca2+ fluctuations modulate the rate of neuronal migration. *Neuron*, **17**, 275–285.
34. Bolteus, A.J. and Bordey, A. (2004) GABA release and uptake regulate neuronal precursor migration in the postnatal subventricular zone. *J. Neurosci.*, **24**, 7623–7631.
35. Farhan, S.M., Wang, J., Robinson, J.F., Prasad, A.N., Rupar, C.A., Siu, V.M., Consortium, F.C. and Hegele, R.A. (2015) Old gene, new phenotype: mutations in heparan sulfate synthesis enzyme, EXT2 leads to seizure and developmental disorder, no exostoses. *J. Med. Genet.*, **52**, 666–675.
36. Farhan, S.M. and Hegele, R.A. (2014) Exome sequencing: new insights into lipoprotein disorders. *Curr. Cardiol. Rep.*, **16**, 507.
37. DePristo, M.A., Banks, E., Poplin, R., Garimella, K.V., Maguire, J.R., Hartl, C., Philippakis, A.A., del Angel, G., Rivas, M.A., Hanna, M. *et al.* (2011) A framework for variation discovery and genotyping using next-generation DNA sequencing data. *Nat. Genet.*, **43**, 491–498.
38. McKenna, A., Hanna, M., Banks, E., Sivachenko, A., Cibulskis, K., Kernytsky, A., Garimella, K., Altshuler, D., Gabriel, S., Daly, M. *et al.* (2010) The Genome Analysis Toolkit: a MapReduce framework for analyzing next-generation DNA sequencing data. *Genome Res.*, **20**, 1297–1303.
39. Auton, A., Abecasis, G.R., Altshuler, D.M., Durbin, R.M., Abecasis, G.R., Bentley, D.R., Chakravarti, A., Clark, A.G., Donnelly, P., Eichler, E.E. *et al.* (2015) A global reference for human genetic variation. *Nature*, **526**, 68–74.
40. Fu, W., O'Connor, T.D., Jun, G., Kang, H.M., Abecasis, G., Leal, S.M., Gabriel, S., Rieder, M.J., Altshuler, D., Shendure, J. *et al.* (2013) Analysis of 6, 515 exomes reveals the recent origin of most human protein-coding variants. *Nature*, **493**, 216–220.
41. Lek, M., Karczewski, K.J., Minikel, E.V., Samocha, K.E., Banks, E., Fennell, T., O'Donnell-Luria, A.H., Ware, J.S., Hill, A.J., Cummings, B.B. *et al.* (2016) Analysis of protein-coding genetic variation in 60, 706 humans. *Nature*, **536**, 285–291.
42. Adzhubei, I., Jordan, D.M. and Sunyaev, S.R. (2013) Predicting functional effect of human missense mutations using PolyPhen-2. *Curr. Protoc. Hum. Genet.*, Chapter 7, Unit 7.20.
43. Kumar, P., Henikoff, S. and Ng, P.C. (2009) Predicting the effects of coding non-synonymous variants on protein function using the SIFT algorithm. *Nat. Protoc.*, **4**, 1073–1081.
44. Schwarz, J.M., Cooper, D.N., Schuelke, M. and Seelow, D. (2014) MutationTaster2: mutation prediction for the deep-sequencing age. *Nat. Methods*, **11**, 361–362.
45. Hutcheon, B., Fritschy, J.M. and Poulter, M.O. (2004) Organization of GABA receptor alpha-subunit clustering in the developing rat neocortex and hippocampus. *Eur. J. Neurosci.*, **19**, 2475–2487.
46. Wearne, S.L., Rodriguez, A., Ehlenberger, D.B., Rocher, A.B., Henderson, S.C. and Hof, P.R. (2005) New techniques for imaging, digitization and analysis of three-dimensional neural morphology on multiple scales. *Neuroscience*, **136**, 661–680.
47. Scorcioni, R., Polavaram, S. and Ascoli, G.A. (2008) L-Measure: a web-accessible tool for the analysis, comparison and search of digital reconstructions of neuronal morphologies. *Nat. Protoc.*, **3**, 866–876.
48. Schindelin, J., Arganda-Carreras, I., Frise, E., Kaynig, V., Longair, M., Pietzsch, T., Preibisch, S., Rueden, C., Saalfeld, S., Schmid, B. *et al.* (2012) Fiji: an open-source platform for biological-image analysis. *Nat. Methods*, **9**, 676–682.
49. Nijhof, B., Castells-Nobau, A., Wolf, L., Scheffer-de Gooyert, J.M., Monedero, I., Torroja, L., Coromina, L., van der Laak, J.A.W.M., Schenck, A. and Graham, L.J. (2016) A new Fiji-based algorithm that systematically quantifies nine synaptic parameters provides insights into drosophila NMJ morphometry. *PLoS Comput. Biol.*, **12**, e1004823.
50. Jenett, A., Rubin, G.M., Ngo, T.-T.B., Shepherd, D., Murphy, C., Dionne, H., Pfeiffer, B.D., Cavallaro, A., Hall, D., Jeter, J. *et al.* (2012) A GAL4-driver line resource for Drosophila neurobiology. *Cell Rep.*, **2**, 991–1001.